Modeling and Real-Time Estimation of Signal-Dependent Noise in Quantum-Limited Imaging

MARC HENSEL
Hamburg University of Technology
Institute for Vision Systems
Harburger Schloßstraße 20
21079 Hamburg, GERMANY

THOMAS PRALOW
Philips Medical Systems
General X-Ray
Röntgenstraße 24-26
22335 Hamburg, GERMANY

ROLF-RAINER GRIGAT
Hamburg University of Technology
Institute for Vision Systems
Harburger Schloßstraße 20
21079 Hamburg, GERMANY

Abstract: Many established and emerging image processing applications rely on quantum-limited imaging, i.e., imaging in extremely poor illumination. At this, images are corrupted by severe signal-dependent Poisson noise. For optimal noise reduction the noise characteristics must be estimated and integrated into the method. Common noise estimators, however, assume Gaussian noise which is not signal-dependent. In this paper, we describe the modeling process exemplarily for low-dose medical X-ray imaging. In this context, we formulate functional models for detector images and images which have undergone nonlinear white compression prior to further processing. Furthermore, we present a robust estimator for signal-dependent noise suited for real-time applications.

Key–Words: Quantum noise, noise estimation, X-ray imaging, white compression

1 Introduction

There is a broad variety of applications relying on poor lighting conditions, for instance, night vision for driver assistance and low-dose medical X-ray image sequences, also known as fluoroscopy. In the latter, X-ray image sequences are processed and visualized in real-time to guide medical interventions. A prominent example is coronary angiography, where narrowed heart arteries can be detected by insertion and observation of contrast agents and treated in minimally invasive procedures. Typically, a large number of single X-ray images is taken. Hence, very small radiation doses are applied for each image in order to minimize the overall exposure of patients and medical staff—resulting in only a very small number of photons available for image formation.

This so-called quantum-limited imaging is characterized by *severe* and *signal-dependent* Poisson noise. For effective noise reduction, the noise level as function of the signal must be known. However, noise estimators are typically designed for Gaussian noise and do not deal with noise signal-dependency.

This paper is organized as follows: Chapter 2 introduces to image acquisition in X-ray imaging. Chapter 3 describes the noise modeling and verifies its validity for X-ray images. In Chapter 4 we develop a fast noise estimator dealing, inter alia, with signal-dependent noise and the influence of image structure on the estimate. The paper concludes with a short summary in Chapter 5.

2 Image Acquisition

X-ray imaging is based on transmission of illumination through objects rather than reflectivity. In an exposure time interval Δt_E, a X-ray tube radiates a positive number $n_t \in \mathbb{N}$, $0 < n_t[m,n] < \infty$, of photons toward a detector pixel at image location $[m,n]$. When passing through an object, the intensity I of the X-ray beam is attenuated according to

$$I = I_0 \exp\left(-\int_{\mathbf{x}_0}^{\mathbf{x}_1} \mu(\mathbf{x}) d\mathbf{x}\right) \tag{1}$$

with initial intensity I_0, material-specific attenuation μ, and $\mathbf{x} \in [\mathbf{x}_0, \mathbf{x}_1]$ denoting the path of the photons.

In a digital detector, the detected number of photons n_d is mapped to an image intensity. Naturally, the result depends on the mapping as well as the detector's sensitivity to quanta at given energy levels. In practice, we model the resulting *raw image* g_{raw} as being linearly dependent on the number of photons, i.e., with constant detector gain $c_g \in \mathbb{R}^+$ and offset $c_o \in \mathbb{R}_0^+$ incoming radiation is mapped to

$$g_{\text{raw}} = c_g\, n_d + c_o\ . \tag{2}$$

Naturally, raw images are mapped in such way that the gray values g_{raw} are within a given dynamic range, for instance, in $[0, 2^b - 1] \subset \mathbb{N}_0$ for b-bit images. Consequently, as doubling the exposure time Δt_E about

doubles the number n_d of detected photons, c_g is inversely proportional to Δt_E, i.e., $c_g \propto 1/\Delta t_E$.

Typically, intensities in an observed image should be proportional to the thickness of radiated objects. To compensate exponential photon attenuation (1) a logarithmic mapping (*white compression*) is applied to raw images prior to image enhancement and visualization. For this, the device-dependent detector offset is compensated ($c_o = 0$) and the resulting image $g_{\text{lin}} = c_g\, n_d$ is mapped to the gray-valued image according to:

$$g_{\text{log}} = c_{\text{log}}\ \ln\left(g_{\text{lin}} + 1\right) \tag{3}$$

Incrementing g_{lin} avoids the undefined expression $\ln(0)$, but has no significant influence on the vast majority of image pixels as $\ln\left(g_{\text{lin}} + 1\right) \approx \ln\left(g_{\text{lin}}\right)$ holds for $g_{\text{lin}} \gg 1$.

3 Noise Model

Noise in low-dose X-ray images origins from various noise sources. To begin with, X-ray beams sensed at a detector are subject to quantum fluctuations—so-called *quantum* or *Poisson noise*—since radiation emission and attenuation are random processes. This means, even in a static setup the number of photons reaching a detector element in the exposure time Δt_E varies. Further noise sources include, for instance, scattered radiation and system noise. The latter integrates noise originating from the hardware, for example, thermal, shot, and quantization noise. However, in spite of other noise sources, quantum noise is by far the dominant noise in low-dose X-ray imaging [2, 8, 10, 14] and other sources can be neglected [1]. In the literature, figures on the X-ray quanta count per pixel differ and are quantified, for instance, as 10 to 200 [2], 20 to 500 [1], and about 35 on average [4].

3.1 State-of-the-Art

Signal degraded by quantum noise, and hence noise in low-dose X-ray imaging, is commonly modeled by a Poisson distribution [1, 4, 8, 10, 14]. Although Poisson noise does not fit the general concepts of additive and multiplicative noise models well [5], typically, the equivalent additive noise model with zero-mean signal-dependent noise is used. Hence, an observed gray-valued image g with intensities $g[m,n]$ at discrete locations $[m,n] \in \Omega = [0, M-1] \times [0, N-1] \subset \mathbb{N}_0^{M \times N}$ is given by

$$g = s + \eta(s) \tag{4}$$

with local mean $\mu(g[m,n]) = s[m,n]$ and variance $\sigma^2(g[m,n]) = \sigma^2(\eta(s[m,n]))$ being determined by the signal s and noise η, only, respectively.

Aach *et al.* [1] note that while a X-ray beam follows Poisson statistics, noise in observed images has been filtered by the imaging system's transfer function and commonly undergone a nonlinear mapping (white compression).

3.2 Poisson Noise

In the following, we formulate the Poisson noise model for X-ray images and link the model parameter to physical quantities and detector constants of the image acquisition process. For this, we assume the detected number n_d of X-ray quanta to follow a Poisson distribution. Hence, the probability of n_d detected photons in an exposure time interval Δt_E is

$$P_\lambda(X = n_d) = \frac{\lambda^{n_d}}{n_d!}\, e^{-\lambda} \tag{5}$$

with λ denoting the noise-free photon count, that is, $\lambda = E[n_d] = \mu(n_d) = s/c_g$ with uncorrupted intensity s and a detector mapping according to (2) with $c_o = 0$. Because of the Poisson statistics

$$\lambda = \mu = \sigma^2 \tag{6}$$

the quantum noise variance is $\sigma^2(n_d) = s/c_g$.

While (5) models the photon count, observed gray values g result from n_d by scaling (2). By this, the model transforms to hold (see, e.g., [4, 8])

$$g \sim P_\lambda(X = g) \sim c_g\, P_\lambda(X = n_d)\ . \tag{7}$$

Hence, mean $\mu(g) = c_g\, \mu(n_d) = s$ and variance $\sigma^2(g) = c_g^2\, \sigma^2(n_d) = c_g\, s \propto s/\Delta t_E$ of an observed image $g = s + \eta(s)$ are linear in the signal s. These statistical properties have several implications on fluoroscopic images: Noise is signal-dependent with noise standard deviation

$$\sigma_\eta = \sigma(g) = \sqrt{c_g\, s} \propto \sqrt{\frac{s}{\Delta t_E}} \tag{8}$$

increasing with dose, but decreasing with exposure time Δt_E. Moreover, contrast and the signal-to-noise-ratio (SNR) increase with brightness and exposure time when defined as $c = \mu^2/\sigma^2 = s/c_g \propto \Delta t_E\, s$ and $\text{SNR} = \mu/\sigma = \sqrt{s/c_g} \propto \sqrt{\Delta t_E\, s}$, respectively.

3.3 Gaussian Approximation

Above Poisson model is rather impractical for noise reduction methods. For this reason, we model noise in low-dose X-ray images by zero-mean Gaussian noise with signal-dependent variance. In the following, this is justified by quantitative verification that (i) under weak conditions a Poisson distribution can be approximated by a sampled Gaussian distribution and (ii) noise in low-dose X-ray images follows a Gaussian distribution for constant signal $s = s_0$.

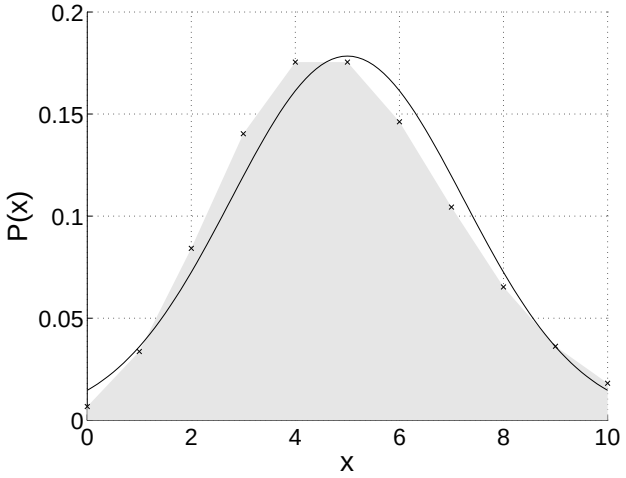

Figure 1: Approximating a Poisson distribution (markers) by the sampled Gaussian distribution (solid line) of same mean and variance $\lambda = 5$. The approximation improves considerably for increasing λ.

3.3.1 Approximating Poisson by Gaussian Distributions

For large $\lambda \gg 1$ the Poisson distribution

$$P_\lambda(X = k) = \frac{\lambda^k}{k!}\, e^{-\lambda} \tag{9}$$

of a discrete random variable X can be approximated by the sampled probability density function of a Gaussian distribution

$$P(X = x; \mu, \sigma^2) = \frac{1}{\sqrt{2\pi}\,\sigma}\, e^{-\frac{(x-\mu)^2}{2\sigma^2}} \tag{10}$$

with same mean and variance $\mu = \sigma^2 = \lambda$:

$$P_\lambda(X = k) \approx \frac{1}{\sqrt{2\pi\lambda}}\, e^{-\frac{(k-\lambda)^2}{2\lambda}} \tag{11}$$

Figure 1 depicts both distributions for $\lambda = 5$. The approximation improves with increasing λ. For a quantitative estimation, the approximation error is analyzed theoretically and numerically.

Theoretic Analysis A theoretical analysis yields the approximation to hold

$$P_\lambda(X = k) = \frac{1}{\sqrt{2\pi\lambda}}\, e^{-\frac{(k-\lambda)^2}{2\lambda}} \cdot O\left(e^{1/\sqrt{\lambda}}\right) \tag{12}$$

for large $\lambda \gg 10$. The detailed derivation is omitted due to limited space, but the idea is sketched as follows: At first, we apply the logarithm $\ln(\cdot)$ and Stirling's formula [7] for large numbers ($k \gg 10$),

$$\ln(k!) \approx \left(k + \frac{1}{2}\right)\, \ln(k) - k + \ln\left(\sqrt{2\pi}\right)\ , \tag{13}$$

to (9). Substitution of observed values k by the components of the additive noise model, i.e., $k = \lambda + \eta$, yields an expression in $\ln(1 + \eta/\lambda)$ which is approximated for $\eta/\lambda \ll 1$ by the Taylor series

$$\ln\left(1 + \frac{\eta}{\lambda}\right) = \frac{\eta}{\lambda} - \frac{1}{2}\left(\frac{\eta}{\lambda}\right)^2 + O\left(\lambda^{-\frac{3}{2}}\right)\ . \tag{14}$$

Finally, substitution $\eta = k - \lambda$ and exponential mapping results in (12).

Numeric Analysis For numeric analysis, the Poisson distribution (9) and its Gaussian approximation (11) as well as the corresponding cumulative probabilities have been compared for discrete $\lambda \in \mathbb{N}$.

Figure 2(a) depicts the maximum approximation errors. The maximum relative approximation error

$$\epsilon_{\text{rel}}[\lambda] = \frac{\max\limits_{k\in\mathbb{N}} \left|P_\lambda(X = k) - P(X = k; \lambda, \lambda)\right|}{\lambda} \tag{15}$$

is about 5.8% at $\lambda = 1$. It drops rapidly with increasing expected mean λ and is below 0.1% for $\lambda \geq 10$. Likewise, the maximum absolute approximation error $\epsilon_{\text{abs}}[\lambda] = \lambda\, \epsilon_{\text{rel}}[\lambda]$ decreases with λ.

Apart from maximum pointwise differences between both probability distributions, we also evaluated the cumulative approximation error. We base our evaluation on the idea of the Kolmogorov-Smirnov (K-S) test, described, for instance, in [16], and quantify the error by differences between the cumulative probability functions $P_\lambda(X \leq x)$ and $P(X \leq x, \mu, \sigma^2)$. While these are identical for minimum and maximum x, as $P(X \leq -\infty) = 0$ and $P(X \leq \infty) = 1$ holds for any distribution P, we measure quality D in terms of the maximum absolute difference in-between:

$$D[\lambda] = \max_{k\geq 0} \left| \sum_{i=0}^{k} \frac{\lambda^i}{i!} e^{-\lambda} - \sum_{i=0}^{k} \frac{e^{-\frac{(i-\lambda)^2}{2\lambda}}}{\sqrt{2\pi\lambda}} \right| \tag{16}$$

Figure 2(b) depicts $D[\lambda]$ according to (16). The function is monotonically decreasing with the maximum error $D[1] = 0.13$.

In summary, for about $\lambda > 10$ a Poisson distribution can be theoretically transformed into a sampled Gaussian distribution with numeric evaluations yielding maximum relative errors below 0.1% and maximum absolute cumulative errors below approximately 0.02. This shows that, at least for $\lambda > 10$, a Poisson distribution $P_\lambda(X = k)$ is approximated well by the sampled Gaussian distribution $P(X = k; \lambda, \lambda)$.

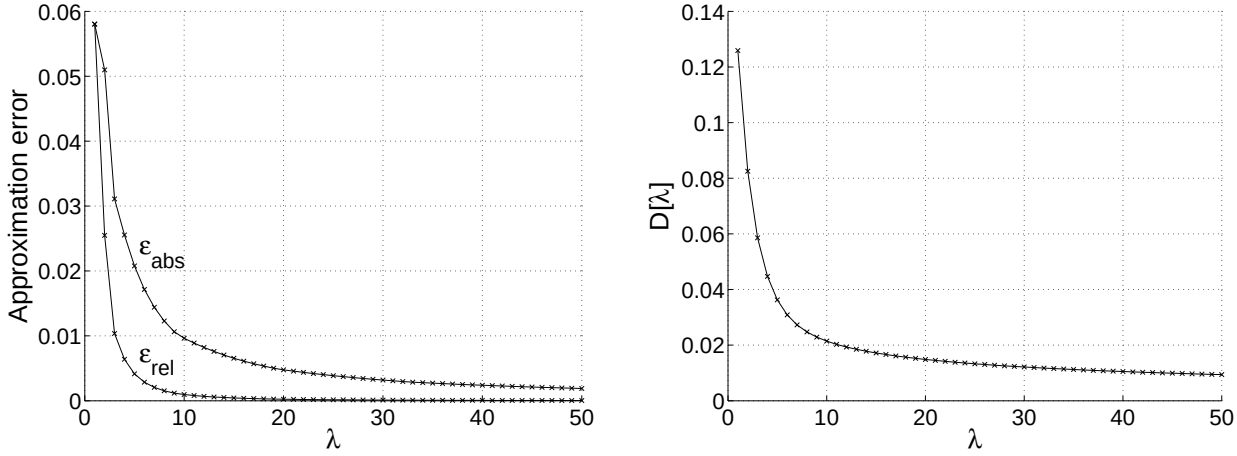

(a) Maximum approximation error

(b) Maximum cumulative approximation error

Figure 2: Approximating a Poisson distribution by the sampled Gaussian distribution of same mean and variance. (a) Probability functions: Maximum absolute and relative errors. (b) Cumulative probability functions: Maximum absolute difference $D[\lambda]$ according to (16) ($k = 2500$).

3.3.2 Characterizing Noise in X-Ray Images by Gaussian Distributions

So far, modeling has been based on theoretical aspects. In the following it is verified that noise in observed X-ray images actually *is* well-approximated by a normal distribution. The test data consists of a non-clinical radiograph containing a large homogeneous area. Prior to evaluation the image has been preprocessed and been subject to rowwise and columnwise normalization in order to, for instance, remove pixel errors and reduce the Heel effect—an intensity gradient caused by self-absorption in X-ray tubes. Preprocessing does not question the validity of the model as we seek to model noise in clinical radiographs where the same preprocessing is applied.

For evaluation, sample mean and standard deviation of a homogeneous area of 1400×2200 pixel have been computed to be $\mu_g = 308.5$ and $\sigma_g = 40.2$ and the area's histogram $h_g[k]$ has been compared numerically to the corresponding Gaussian distribution $P(X = k; \mu_g, \sigma_g^2)$. The maximum absolute error

$$\mathrm{MAE} = \max_{k \in [k_0, k_1]} |h_g[k] - P(X = k; \mu_g, \sigma_g)| \quad (17)$$

and the mean squared error

$$\mathrm{MSE} = \frac{\max\limits_{k \in [k_0, k_1]} \left((h_g[k] - P(X = k; \mu_g, \sigma_g))^2 \right)}{k_1 - k_0 + 1} \quad (18)$$

have been assessed in the dynamic range, i.e., for $k \in [k_0, k_1] \subset \mathbb{N}_0$ with $h_g[k_0] \neq 0$, $h_g[k_1] \neq 0$, and $h_g[k] = 0$ for $k \notin [k_0, k_1]$. Both measures yield low errors of $\mathrm{MAE} = 1.57 \cdot 10^{-4}$ and $\mathrm{MSE} = 1.26 \cdot 10^{-9}$, respectively.

Moreover, a Kolmogorov-Smirnov test has been applied. In the evaluation of a data set containing N samples with the empiric cumulative probability function $P_N(X \leq x)$ against a given distribution $P(X \leq x)$, the significance level of

$$D = \max_{-\infty < x < \infty} |P_N(X \leq x) - P(X \leq x)| \quad (19)$$

as disproof of the null hypothesis that the distributions P_N and P are identical is approximately [16]

$$\text{Probability}(D > \text{observed}) = Q_{\mathrm{KS}} \left(\sqrt{N} D \right) \quad (20)$$

with the monotonic function

$$Q_{\mathrm{KS}}(\alpha) = 2 \sum_{j=1}^{\infty} (-1)^{j-1} \exp\left(-2 j^2 \alpha^2\right) . \quad (21)$$

For the test, typical values of $N = 40$ samples and a significance level of 5% were chosen. The K-S test verified the null hypothesis that the X-ray image follows the distribution $P(X = x; \mu_g, \sigma_g^2)$. This is a strong indicator that noise in observed X-ray images can be assumed to be Gaussian-distributed.

3.4 White Compression

In Section 3.2, noise standard deviation in the Poisson noise model has been derived to hold $\sigma(g) = \sqrt{c_g \, s}$. In the following we estimate the effect of the logarithmic mapping (3) on the signal-dependent noise level. To simplify expressions, we assume $g \gg 1$, which

justifies the approximation $\ln(g+1) \approx \ln(g)$. With s and η denoting signal and noise in the linear detector image $g_{\text{lin}} = s+\eta$, the corresponding observed image $g_{\log}$ is given by:

$$g_{\log} = c_{\log} \ln(s+\eta(s)) \quad (22)$$

$$= c_{\log} \left(\ln(s) + \ln\left(1 + \frac{\eta(s)}{s}\right)\right) \quad (23)$$

The signal-dependent noise level of the logarithmized data is $\sigma_{\log} = \sigma(g_{\log})$. As $\ln(s)$ is constant, this is equivalent to

$$\sigma_{\log} = c_{\log} \cdot \sigma\left(\ln\left(1 + \frac{\eta(s)}{s}\right)\right) . \quad (24)$$

The statistical properties of the term η/s can be expressed when regarding $\mu(\eta) = 0$, $\sigma^2(\eta) = c_g\, s$, and $\lambda = s/c_g$:

$$\mu\left(\frac{\eta}{s}\right) = \frac{\mu(\eta)}{s} = 0 \quad (25)$$

$$\sigma\left(\frac{\eta}{s}\right) = \sqrt{\frac{\sigma^2(\eta)}{s^2}} = \frac{1}{\sqrt{\lambda}} \quad (26)$$

In other words, η/s is of order $\lambda^{-1/2}$ and $\eta/s \ll 1$ holds for large $\lambda \gg 1$.

To evaluate $\sigma_{\log}$, the term $\ln(1+\eta/s)$ is approximated by the Taylor series

$$T_n(x) = \sum_{k=1}^{n} \frac{(-1)^{k+1}}{k} \cdot x^k \quad (27)$$

for $f(x) = \ln(1+x)$ at location $x_0 = 1$. The series is a good approximation for $|x| \ll 1$ which is fulfilled in our case. By using the linear Taylor approximation $T_1(\eta/s) = \eta/s$ of $\ln(1+\eta/s)$ the noise level (24) is approximated by:

$$\sigma_{\log} = c_{\log}\, \sigma\left(\frac{\eta}{s}\right) = \frac{c_{\log}}{\sqrt{\lambda}} = c_{\log} \sqrt{\frac{c_g}{s}} \quad (28)$$

Finally, (3) is applied to signal s along with observed gray values. Consequently, noise should be a function of $s_{\log} = c_{\log} \ln(s+1) \approx c_{\log} \ln(s)$, which is equivalent to $s = \exp(s_{\log}/c_{\log})$, rather than s:

$$\sigma_{\log} = c_{\log} \sqrt{c_g} \exp\left(-\frac{s_{\log}}{2c_{\log}}\right) \quad (29)$$

In summary, white compression according to the logarithmic mapping (3) transforms the noise characteristics and the signal-dependent noise $\sigma_{\log}(s_{\log})$ can be modeled as monotonically decreasing exponential function (29). Again, this model has been verified using non-clinical X-ray images.

4 Noise Estimation

Noise reduction as well as contrast enhancement methods can be significantly improved by consideration of the signal-dependent noise level. For this, the quantitative dependency of the noise level σ from the signal s must be know, i.e., we require an estimation of the signal-dependent noise curve $\sigma(s)$.

4.1 State-of-the-Art

Typically, noise estimation methods assume additive, uncorrelated, stationary, zero-mean Gaussian white noise—and assume it to be not signal-dependent.

In a comparison of various approaches, Olsen [15] found that, on average, *prefiltering* generates the most reliable estimate. In this approach an observed image $g = s + \eta$ is filtered to reduce the influence of structure. More precisely, filtering g yields an estimate $s_e = \text{filter}(g) \approx s$ of the signal and the difference $\eta_e = g - s_e$ between observed gray value g and estimated signal s_e is interpreted as noise component. The estimated noise level is thus given by σ_{η_e} using the sample variance $\sigma^2_{\eta_e} = \mathrm{E}[(\eta_e - \mathrm{E}[\eta_e])^2]$.

Common prefilters are binomial and median filters. Binomial filtering models s to be planar within the filter window—which is not fulfilled at edges, resulting in a tendency to overestimate noise [3]. For this reason, commonly edge pixels are disregarded based on the 1st or the 2nd derivation [9, 12]. Typically, only pixels with a gradient below a threshold, $\|\nabla g\| < \tau \in \mathbb{N}$, or only p percent of pixels with lowest gradients contribute to the estimate [3, 15]. In contrast, median filters allow the image model to contain structure like step edges. All pixels contribute to the estimate and no gradients are required. Rank *et al.* [17] found the best window size of smoothing filters to be, at large, 3×3 pixel.

Other common approaches estimate noise in homogeneous image regions as these are likely not to contain structure falsifying the result. For instance, block-based methods typically average the smallest standard deviations in image blocks [3]. Bosco *et al.* [6] propose a fast method based on local pixelwise differences. If all differences are below a threshold, a homogeneous area is assumed and the noise level is estimated from the noise histogram. Other histogram approaches include, for instance, [17].

4.2 Approach

Most state-of-the-art noise estimation methods are not valid for X-ray imaging as the assumption of signal-independent noise is not fulfilled. Moreover, methods must be fast to be applicable for real-time fluoroscopy. While there are fast prefiltering and block-based noise

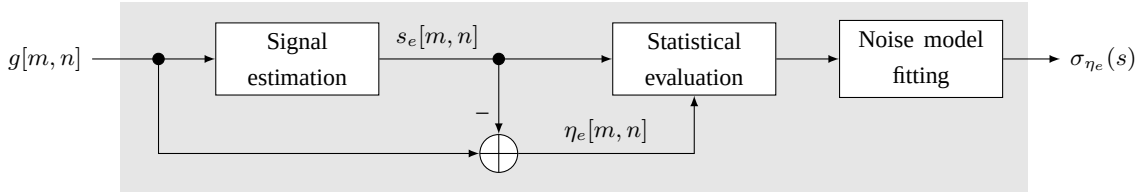

Figure 3: Noise estimation by prefiltering

estimators, the latter is not well suited for medical X-ray imaging. First of all, there is no *a priori* knowledge if and where there are homogeneous blocks with $s \in [s_0 - ds, s_0 + ds]$ and small ds in an image. Furthermore, blocks for *all* signal levels would be required to estimate the signal-dependent noise levels—a requirement that will hardly be fulfilled in practice.

Hence, we chose a prefiltering approach depicted in Figure 3. Following signal estimation s_e, the noise component at location $[m, n]$ is estimated to be

$$\eta_e[m,n] = g[m,n] - s_e[m,n] \ . \tag{30}$$

The signal-dependent noise curve $\sigma_{\eta_e}(s)$ follows from a statistical evaluations of all noise components at identical estimated signal levels s_e, i.e.,

$$\sigma^2_{\eta_e}(s) = \mathrm{E}\left[(\eta_e(\Omega_s) - \mathrm{E}[\eta_e(\Omega_s)])^2\right] \tag{31}$$

$$= \frac{\sum\limits_{[m,n]\in\Omega_s} (\eta_e[m,n] - \mu_{\eta_e}(s))^2}{|\Omega_s| - 1} \tag{32}$$

with

$$\Omega_s = \{\ [m,n] \mid s_e[m,n] = s\ \}\ , \tag{33}$$

spatial domain $\Omega = \bigcup_s \Omega_s$, $|\Omega_s|$ denoting the number of elements in Ω_s, and sample mean

$$\mu_{\eta_e}(s) = \frac{1}{|\Omega_s|} \sum_{[m,n]\in\Omega_s} \eta_e[m,n] \ . \tag{34}$$

Finally, postprocessing increases the reliability of the estimate and fits the data to the noise model.

A drawback of prefiltering is that η_e contains signal components if $s_e[m,n] \neq s[m,n]$. For this reason, the problem has to be addressed, how to filter g in such way that s_e resembles s as closely as possible or at least that the sample variance of $\eta_e = g - s_e$ resembles noise variance. In accordance with the state-of-the-art, 3×3 binomial and median filters are taken into account for signal estimation. Binomial filters h are well suited to attenuate Gaussian noise. Thus, one can expect $\eta_e = g - h * s$ to contain a great extent of the noise. However, linear filtering cannot separate noise and structure and thus η_e will contain significant components representing object structure. Median filters, on the other hand, are not as suited to reduce Gaussian noise, but exhibit better structure preservation. Thus, one can expect η_e to contain less Gaussian noise, but also to contain less structure falsifying the result.

There are three main issues, to be discussed in the following sections: How do the filters perform when there is no structure present, i.e., in uniform signal $s[m,n] = s_0 \in \mathbb{N}_0$? How do the filters perform in the presence of structure? And finally, how can falsifications due to structure be reduced?

4.3 Prefilters for Uniform Signal

To begin with, we analyze noise estimation without the influence of image structure. An observed image $g[m,n] = s_0 + \eta[m,n]$ is modeled to consist of uniform signal $s_0 \in \mathbb{N}_0$ and uncorrelated zero-mean Gaussian noise η with standard deviation $\sigma_0 \in \mathbb{R}^+$. Noise estimation performance is measured by the relative estimation error

$$\epsilon_{\eta_e} = \frac{\sigma_{\eta_e} - \sigma_0}{\sigma_0} \tag{35}$$

of the estimated noise σ_{η_e} with regard to the true noise level σ_0 in the image. In uniform signal the estimated noise is expected to be always slightly below the true noise, i.e., $\epsilon_{\eta_e} < 0$. This is due to signal estimation as filtering does not yield constant $s_e[m,n] = s_0$, thus, some of the noise energy is estimated to be signal.

Noise estimation performance using binomial filtering, i.e., linear filtering $s_e = h * g$ with filter mask h, can be derived theoretically when assuming noise statistics to be independent from the location $[m,n]$ and signal $s[m,n]$. The variance of a weighted sum $X = \sum_i c_i X_i$ of independent Gaussian variables X_i with variances σ_i^2 is given by

$$\sigma^2(X) = \sum_i c_i^2\ \sigma_i^2 \ . \tag{36}$$

Hence, as linear filtering yields weighted sums of pixels $g[m,n]$ with independent Gaussian noise σ_0^2, the noise variance in the filtered image holds

$$\sigma^2_{s_e} = \sum_{i,j} h[i,j]^2\ \sigma_0^2 \ . \tag{37}$$

Filter	Size	σ_{s_e}/σ_0 [%]	σ_{η_e}/σ_0 [%]	ϵ_{η_e} [%]
Median (measured)	3×3	40.81 ± 0.05	97.13 ± 0.04	-2.87 ± 0.04
Binomial (derived)	3×3	37.50	80.04	-19.96
	5×5	27.34	89.08	-10.92
	7×7	22.56	92.50	-7.50

Table 1: Noise estimation performance in uniform signal. (a) Median filter: Average (accuracy, bias) and standard deviation (precision, non-systematic error) of 100 measurements in test images containing 1024×1024 pixel ($s_0 = 0$, $\sigma_0 = 100$, no clipping). (b) Binomial filters: Derived according to (37) and (38).

Likewise, estimated noise components $\eta_e = g - s_e = g - (h * g)$ are weighted sums of pixels $g[m, n]$, however, differing in the central weight. With $\delta[\cdot]$ denoting the Kronecker function, noise variance is given by

$$\sigma_{\eta_e}^2 = c_h \, \sigma_0^2 \tag{38}$$

with

$$c_h = \sum_{i,j} (1 - \delta[i]\delta[j]) \, h[i, j]^2 + (1 - h[0, 0])^2 \tag{39}$$

and the relative error holds $\epsilon_{\eta_e} = c_h - 1$. For median filtering, we determined noise in estimated signal s_e and noise components η_e as well as the relative error ϵ_{η_e} by numerical simulations.

Table 1 summarizes the results. Although it has been stated (e.g., [13]) that median filters are not suited to reduce Gaussian noise, Boncelet [5] notes that these perform only slightly worse in Gaussian noise than linear averaging. This is supported by the results in Table 1. Regarding 3×3 filters, i.e., the preferred filter size for noise estimation, about 40.8% and 37.5% of the noise standard deviation σ_0 remains in s_e after filtering with median and binomial filters, respectively. However, the statistical properties in $\eta_e = g - s_e$ reflect the noise level σ_0 by far better in case of median filtering, yielding an absolute relative error $|\epsilon_{\eta_e}|$ of about 2.9% compared to 20.0% for binomial filtering.

4.4 Prefilters in the Presence of Structure

So far, we have analyzed noise estimation performance in constant signal $s[m, n] = s_0$, for instance, homogeneous areas. In natural images, though, signal inhomogeneities like edges affect the estimate. A prefilter yields a signal estimate, which typically is not identical to the signal, i.e., $s_e \neq s$. Consequently, signal structure falsifies the estimated noise component $\eta_e = g - s_e \neq \eta$ and hence noise standard deviation σ_{η_e} calculated from η_e. As illustrated in Figure 4, the additional components η_e due to structure tend to have negative sign for small signal s_e and positive sign for large signal.

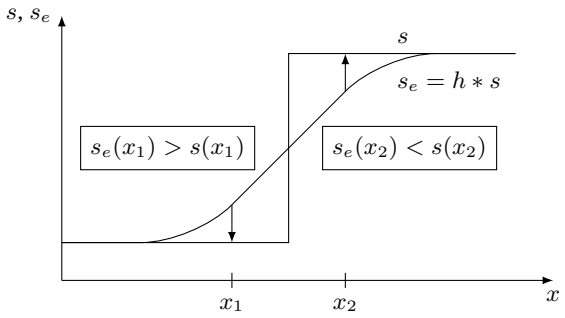

Figure 4: Predominant signs of falsifications due to structure. A step edge s is smoothed for signal estimation s_e. At the lower (left) side of the edge s, the estimated signal is $s_e > s$. Thus, the estimated noise $\eta_e = s - s_e$ is negative. The opposite is true for the larger (right) side of the edge.

4.4.1 Iterative Outlier Removal

As discussed above, state-of-the-art prefiltering methods typically address the problem (i) by disregarding locations with intensity gradient $\|\nabla g\|$ above a threshold $\tau \in \mathbb{N}$ or (ii) by evaluating p percent of pixels with lowest entries in an edge image, only. We propose a third approach based on the *a priori* knowledge that the noise components $\eta[m, n]$ are expected to be Gaussian-distributed, i.e., about 99.7% of the samples are in the 3σ interval of the distribution. Thus, there is a high probability that values outside this interval are dominated by structure rather than noise. To reduce falsifications due to structure, we remove these outliers from the sample set and update the estimated standard deviation using the remaining samples. That is, for each signal level s, starting from an initial sample set $\eta_e[\mathbf{m}]$ at locations $\mathbf{m} = [m, n] \in \Omega_s^{(0)}$,

$$\Omega_s^{(0)} = \{ \, \mathbf{m} \mid s_e[\mathbf{m}] = s \, \} \ , \tag{40}$$

and noise estimate

$$\sigma_{\eta_e}^{(0)}(s) = \mathrm{E}\left[\left(\eta_e \left(\Omega_s^{(0)} \right) - \mathrm{E}\left[\eta_e \left(\Omega_s^{(0)} \right) \right] \right)^2 \right]^{1/2} \tag{41}$$

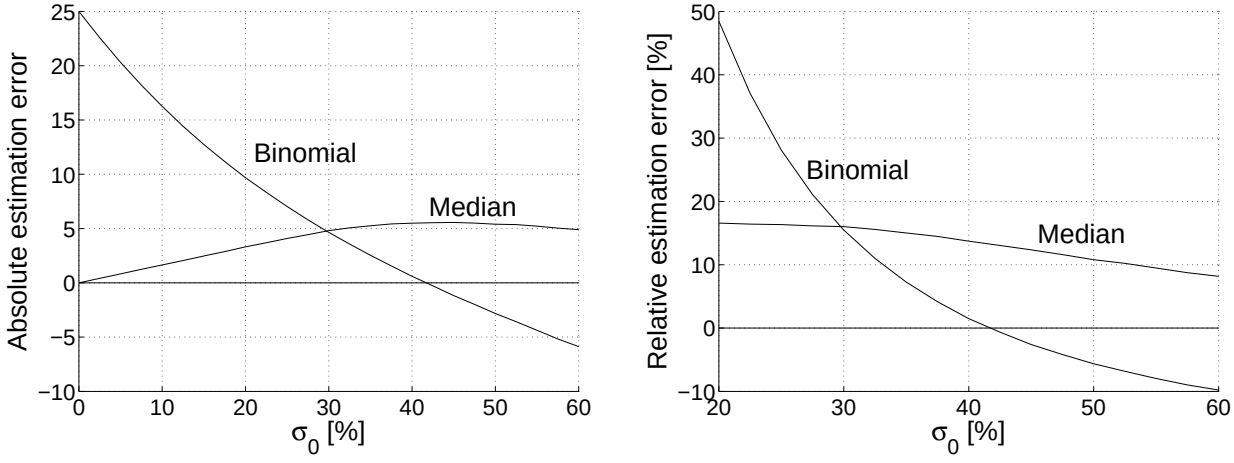

(a) Absolute error $\sigma_0\epsilon_{\eta_e}$ (b) Relative error ϵ_{η_e}

Figure 5: Noise estimation performance at corrupted edges. The 1024×1024 pixel test signal contains 2 pixel wide vertical bars with $s_0 = 0$ and $s_1 = 100$. Zero-mean Gaussian noise with standard deviations σ_0 (in percentage of step size $\Delta s = s_1 - s_0$) has been added and noise estimated using 3×3 median and binomial filters. (a) Absolute errors. (b) Relative errors ($\sigma_0 \geq 20$ as relative errors are very large for smaller noise in binomial filtering).

according to (31) to (33), in each iteration step the sample set is reduced to

$$\Omega_s^{(k+1)} = \left\{ \mathbf{m} \,\middle|\, \eta_e[\mathbf{m}] \in \Omega_s^{(k)} \wedge |\eta_e[\mathbf{m}]| \leq 3\sigma_{\eta_e}^{(k)}(s) \right\} \tag{42}$$

and the standard deviation $\sigma_{\eta_e}^{(k+1)}(s)$ updated appropriately.

Our experiments show that this method is superior to state-of-the-art gradient-based approaches. A general problem when integrating gradients or edge detection (e.g., [9]) into noise estimation is that these are very sensitive to noise. In particular in strong noise, strongly corrupted pixels are omitted from the estimation while edges might be comparatively weak and hence contribute to the estimate.

4.4.2 Influence of Edges

We begin the analysis of the effect of structure on the noise estimation by 3×3 median and binomial prefiltering with some considerations on ideal step edges. In the noise-free case, $g = s$, median filters preserve edges, $s_e = \text{median}_{3\times3}(s) = s$, and hence these do not falsify noise estimates σ_{η_e}. Binomial filtering, on the other hand, blurs edges, $s_e = h * s \neq s$, and falsifies σ_{η_e}. In the presence of noise, $g = s+\eta$, median as well as binomial filters affect σ_{η_e}. In case of binomial filters, signal components s are blurred in estimated signal due to $s_e = h * (s + \eta) = h * s + h * \eta$. In median filtering, this results from the fact that the median of *all* pixels in the filter window is chosen while the median of pixels of the homogeneous area containing the center pixel is desired. This introduces a slight bias toward the "other" intensity level of the edge.

The influence of ideal step edges corrupted by noise has been assessed in numerical simulations. The test signal contains vertical bars with intensities s_0 and $s_1 > s_0$. Each bar is 2 pixels wide so that exactly one edge is contained in a 3×3 filter window at every location. Figure 5 depicts the absolute and relative noise estimation errors $\sigma_0\epsilon_{\eta_e}$ and ϵ_{η_e} in dependency of the true noise level σ_0. Note that the relative error is not plotted for $\sigma_0 < 20$ as relative errors can take excessively large values for small σ_0 [17]—which is the case for binomial filtering in this simulation. In median filtering, noise is slightly overestimated ($\epsilon_{\eta_e} > 0$) regardless of σ_0. In the case of binomial filtering underestimation occurs for noise larger than approximately $\sigma_0 \approx 42\%$ of the step height $\Delta s = s_1 - s_0$.

Olsen [15] notes that noise should be overestimated in the presence of structure and underestimation might occur when noise is driven into saturation. This general tendency need not be true for very hight noise levels σ_0 as prefiltering underestimates noise in the absence of structure, for instance, by about 20% for 3×3 binomial filtering (Table 1). This component becomes dominant with increasing σ_0.

4.4.3 Influence of Clinical Structure

We repeated above experiments with a clinical image. For numerical simulations, we chose an image of size 1024×1024 pixel showing a vessel tree filled with contrast agent as this contains clinical relevant struc-

ture of varying sizes. In order to obtain an almost noise-free clinical reference image, noise has been reduced by computational complex nonlinear diffusion filtering.

For the evaluation, Gaussian noise with standard deviation σ_0 has been first added to and afterwards estimated from the image. Apart from low noise levels where—as explained above—the measure is not meaningful, the relative estimation error ϵ_{η_e} is roughly constant throughout the analyzed noise levels. For σ_0 in 5% to 60% (step size: 2.5%) of the maximum image intensity, median filtering yielded a mean relative error of -2.85% with a standard deviation of 0.05%. Binomial filtering resulted in $-19.92\% \pm 0.09\%$. The magnitudes are hence within the errors of the noise-free case according to Table 1.

5 Summary and Conclusion

To this day, literature on noise modeling and estimation concentrates on signal-independent Gaussian noise. In this paper, we have presented modeling for signal-dependent quantum noise occurring in important and established applications as, for instance, low-dose medical X-ray imaging. At this, our contributions include, in particular, modeling the effect of typical nonlinear mappings and establishing a link to physical quantities like the exposure time.

Moreover, we presented a robust and fast estimator for signal-dependent Gaussian noise with high performance in, both, homogeneous areas and natural clinical structure. Inter alia, it has shown that, in spite of its inferiority regarding the reduction of Gaussian noise, at large, prefiltering by a 3×3 median filter clearly outperforms 3×3 binomial prefiltering. All results are also valid for noise that is not signal-dependent and the noise estimator can easily be adapted for such applications.

Modeling as well as noise estimation are a requisite of utmost importance in order to yield considerable structure-preserving noise reduction. For this reason, the results presented in this paper are the basis of the noise reduction methods (e.g., [11]) developed by our research groups for clinical application.

References:

[1] T. Aach, D. Kunz, R. Florent, and S. Makram-Ebeid, Noise Reduction and Image Enhancement Algorithms for Low-Dose X-Ray Fluoroscopy, *Proc. BVM*, 1996, pp. 95–100.

[2] T. Aach and D. Kunz, Multiscale Linear/Median Hybrid Filters for Noise Reduction in Low Dose X-Ray Images, *Proc. ICIP* 2, 1997, pp. 358–361.

[3] A. Amer and E. Dubois, Fast and Reliable Structure-Oriented Video Noise Estimation, *IEEE Trans. on Circuits and Systems for Video Technology* 15, 2005, pp. 113–118.

[4] R. Aufrichtig and D.L. Wilson, X-Ray Fluoroscopy Spatio-Temporal Filtering with Object Detection, *IEEE Trans. on Medical Imaging* 14, 1995, pp. 733–746.

[5] C. Boncelet, Image Noise Models, In: A.C. Bovik (Edt.), *Handbook of Image and Video Processing*, 2nd edt., Elsevier Academic Press, 2005, pp. 397–409.

[6] A. Bosco, A. Bruna, G. Messina, and G. Spampinato, Fast Method for Noise Level Estimation and Denoising, *Proc. ICCE*, 2005, pp. 211–212.

[7] I.N. Bronstein, K.A. Semendjajew, G. Musiol, and H. Mühlig, *Taschenbuch der Mathematik*, 6th edt., Verlag Harri Deutsch, 2005.

[8] C.L. Chan, A.K. Katsaggelos, and A.V. Sahakian, Image Sequence Filtering in Quantum-Limited Noise with Applications to Low-Dose Fluoroscopy, *IEEE Trans. on Medical Imaging* 13, 1993, pp. 610–621.

[9] B.R. Corner, R.M. Narayanan, and S.E. Reichenbach, Noise Estimation in Remote Sensing Imagery Using Data Masking, *Intern. Journal of Remote Sensing* 24, 2003, pp. 689–702.

[10] R.J. Ferrari and R. Winsor, Digital Radiographic Image Denoising via Wavelet-Based Hidden Markov Model Estimation, *Journal of Digital Imaging* 18, 2005, pp. 154–167.

[11] M. Hensel, T. Pralow, and R.-R. Grigat, Real-Time Denoising of Medical X-Ray Image Sequences: Three Entirely Different Approaches, *Proc. ICIAR*, 2006, pp. 479–490.

[12] J. Immerkær, Fast Noise Variance Estimation, *CVIU* 64, 1996, pp. 300–302.

[13] B. Jähne, *Digital Image Processing*, 6th edt., Springer, 2005.

[14] D. Kunz, K. Eck, H. Fillbrandt, and T. Aach, A Nonlinear Multi-Resolution Gradient Adaptive Filter for Medical Images, *SPIE Medical Imaging* 5032, 2003, pp. 732–742.

[15] S.I. Olsen, Estimation of noise in images: An evaluation, *CVGIP: Graphical Models and Image Processing* 55, 1993, pp. 319–323.

[16] W.H. Press, B.P. Flannery, S.A. Teukolsky, and W.T. Vetterling, *Numerical Recipes in C*, 2nd edt., Cambridge University Press, 1992.

[17] K. Rank, M. Lendl, and R. Unbehauen, Estimation of Image Noise Variance, *Proc. Vision, Image and Signal Processing* 146, 1999, pp. 80–84.